Available online at www.sciencedirect.com
SCIENCE DIRECT®
International Journal of Multiphase Flow 31 (2005) 416–434
International Journal of Multiphase Flow
www.elsevier.com/locate/ijmulflow

Reynolds number dependence of gas-phase turbulence in gas–particle flows

K. Hadinoto *, E.N. Jones, C. Yurteri, J.S. Curtis

School of Chemical Engineering, Purdue University, West Lafayette, IN 47907, USA

Received 19 November 2003; received in revised form 4 November 2004

Abstract

A downward flow of glass bead particles in a vertical pipe is investigated using a two-component LDV/PDPA for a range of *Re* ($6400 < Re < 24{,}000$) and a constant particle loading ($m = 0.7$). Two particle sizes of 70 and 200 μm are considered in the present work. For the 70 μm particles, the presence of the particles dampens the gas-phase turbulence intensity at the lowest value of *Re* investigated (8300) compared with the single-phase flow at the same *Re*. As *Re* increases, the gas turbulence increases, and for $Re > 13{,}800$ the gas turbulence is enhanced compared with the single-phase flow at the same *Re*. For the 200 μm particles, the intensity also increases with *Re* and is enhanced for all values of *Re* investigated, except at the lowest value of *Re* investigated (6400). At this value, the gas turbulence is equal to that of single-phase flow at the same *Re*. The observed trend in the gas-phase turbulence modulation with *Re* is proposed to be due to the change in the segregation patterns and in the average volume fractions of the particles with increasing *Re*. More importantly, the present experimental results suggest that, consideration of either the gas and particle characteristic length scales or the particle Reynolds number solely is insufficient to predict gas-phase turbulence modulation in gas–particle flows.

Keywords: Gas–particle flow; Granular flow; Reynolds number; Turbulence modulation; LDV

* Corresponding author. Tel.: +1 765 494 4055; fax: +1 765 494 0805.
E-mail address: hadinoto@ecn.purdue.edu (K. Hadinoto).

0301-9322/$ - see front matter © 2004 Elsevier Ltd. All rights reserved.
doi:10.1016/j.ijmultiphaseflow.2004.11.009

1. Introduction

Turbulent gas–particle flow occurs in many industrial applications, such as in pneumatic transport of particulates, circulating fluidized beds, cyclone separators and chemical reactors. Interactions between the particles and the gas lead to the changes in the level of the gas-phase turbulence intensity. A number of factors known to influence the gas-phase turbulence modulation in a gas–particle flow system have been studied extensively. These factors include particle size, particle density, and particle loading m, defined as the ratio of the particle mass flow rate to the gas mass flow rate

$$m = \frac{\int_{A_c} \rho_s \upsilon U_s \, dA_c}{\int_{A_c} \rho_f (1-\upsilon) U_f \, dA_c} \tag{1}$$

where U_s, U_f, ρ_s and ρ_f are the time-averaged axial velocity and the density of the particle and the gas, respectively, υ is the particle volume fraction and A_c is the cross-sectional area of the flow. Some of the key results from a number of these studies are summarized in the present section.

Maeda et al. (1980) studied the effect of particle size in a turbulent gas–particle upward pipe flow with glass beads ranging in size from 45 to 136 μm at $Re = 20{,}000$. They found an increase in the two-phase gas-phase turbulence intensity for all particle sizes investigated compared to single-phase flow. Lee and Durst (1982) conducted a similar study with larger size particles at $Re = 8000$ and showed that 800 μm glass beads increased the gas-phase turbulence intensity over the entire pipe cross-section. In a similar study, Tsuji et al. (1984) employed polystyrene particles and measured axial mean and fluctuating velocities of both the gas and particle phase at several Re ($Re = 16{,}700$, 22,700, 26,900, 30,600, 39,600). They considered different particle sizes (200 μm to 3 mm) and varied the particle loadings up to five. The specific particle loadings investigated (and also the particle sizes in some cases) were different for each Re. Both enhancement of the gas turbulence in the presence of large particles, and attenuation in the presence of the smallest particles, were observed. An increase in the particle loading for the smaller particles (<500 μm) resulted in a further decrease of the gas turbulence intensity. For larger particles that enhanced the gas turbulence intensity, increases in the particle loading led to further increases in the gas turbulence. Despite differences in the particle density and the particle loading employed in their respective experiments, the experimental results of Tsuji et al. (1984) at $Re = 16{,}700$ for particles greater than 500 μm were in agreement with the results of Lee and Durst (1982). In both cases, gas turbulence enhancement was observed in the presence of larger particles. However, the experimental results of Maeda et al. (1980) were in contrast to these results, showing gas turbulence enhancement with much smaller particles but at a Reynolds number higher than in either the Tsuji et al. or the Lee and Durst experiments.

Hardalupas et al. (1989) studied the effect of particle loading on the relative velocity of a downward particle-laden jet at $Re = 13{,}000$. For 80 μm particles at particle loadings of 0.23 and 0.86, they observed a decrease in the slip velocity with increasing particle loading and a sign change near the pipe wall at the exit of the nozzle. Kulick et al. (1994) studied the effect of particle density on a turbulent vertical air channel flow with 50 and 90 μm glass beads particles and 70 μm copper spherical particles at $Re = 13{,}800$. Although the mean gas velocity profiles were not affected by the presence of the particles, the axial and radial gas fluctuating velocities were found to be

attenuated by the presence of the particles, with the degree of attenuation due to the glass particles found to be greater than that of copper particles at the same particle loading. In this study, as well as all previous studies on turbulence modulation to date, the experiments were conducted at a constant *Re*. The effect of changing the *Re*, while maintaining other variables constant, was not investigated.

Gore and Crowe (1989) and Hetsroni (1989) sought to summarize the effects of the particles on the fluid turbulence by compiling fluid–particle flow data available in the literature at that time. Gore and Crowe (1989) suggested a demarcation criterion for enhancement or suppression of the fluid turbulence in the presence of the particles, based solely on the characteristic length scales of both phases and independent of the *Re*. This critical parameter was proposed to be the ratio d_p/l_e, where d_p is the particle diameter and l_e is the characteristic length of the most energetic eddy. In order to estimate l_e, Gore and Crowe applied the work of Hutchinson et al. (1971), which showed that the ratio l_e/R, where R is the pipe radius, was approximately constant across the pipe cross-section ($l_e/R = 0.2$) and independent of *Re* based on results at $Re = 50{,}000$ and $Re = 500{,}000$.

As mentioned before, the data sets for the gas–particle flows compiled by Gore and Crowe (1989) maintained a constant *Re* and varied the particle size, particle density and/or particle loading. For small particles ($d_p/l_e \leqslant 0.1$), Gore and Crowe (1989) reasoned that the particles would travel with the most energetic gas eddies, resulting in diminished gas turbulent kinetic energy resulting from the fluctuating drag force used to transport the particles. On the other hand, larger particles ($d_p/l_e > 0.1$) could enhance gas turbulence by the presence of vortex shedding behind the particles, thus taking energy from the mean motion of the gas and transferring it to the gas turbulent kinetic energy. Hetsroni (1989) reasoned that the key parameter describing the vortex shedding phenomena was the particle Reynolds number Re_p,

$$Re_p = \frac{\rho_f d_p |U_f - U_s|}{\mu_f} \tag{2}$$

where μ_f is the gas viscosity. Hetsroni (1989) showed that $Re_p > 400$ was sufficient for vortex shedding to occur. Neither the Gore and Crowe (1989) nor the Hetsroni (1989) criteria, however, are sufficient to explain the gas turbulence enhancement observed by Maeda et al. (1980) in the presence of smaller particles. Applying these criteria for turbulence enhancement to the 45 μm data of Maeda et al. (1980) at a $Re = 21{,}000$, one finds that d_p/l_e is approximately 0.008, much less than the $d_p/l_e = 0.1$ demarcation as proposed by Gore and Crowe (1989). The Re_p is approximately 1.2, which is also much less than the $Re_p = 400$ demarcation as proposed by Hetsroni (1989).

Best (1998) also studied fluid turbulence enhancement for low and moderate particle Reynolds numbers ($Re_p < 300$) in a recirculating flume. This work suggested that particle rotation can greatly influence the flow pattern around large particles, particularly near the wall where both particle–wall collisions are important and higher particle concentrations are present. If particle rotation is present, Best (1998) suggested that fluid turbulence enhancement might occur at a much lower Re_p than previously suggested by Hetsroni (1989).

This paper presents experimental results from a study specifically designed to examine the *Re* dependence of gas-phase turbulence modulation in the presence of particles. In order to achieve this objective, turbulent gas–particle flow is studied at a constant particle loading for a wide range of *Re*. LDV/PDPA measurements are obtained and analyzed for two sizes of particles, 70 μm and

200 μm glass beads. The results from this study are also used to evaluate the demarcation criteria for enhancement or suppression of gas turbulence as originally proposed by Gore and Crowe (1989) and Hetsroni (1989).

2. Experimental setup

The two-phase system employed in the present work involves gas and particles flowing vertically downward in a pipe. The particles are spherical (>85% perfect spheres) glass beads with arithmetic mean diameters of 70 and 200 μm, available commercially from the Mo-Sci Corporation. Greater than 80% of the beads are in their designated size range, which is 62–88 μm for the 70 μm particles and 177–250 μm for the 200 μm particles. Glass spheres with diameters of less than 5 μm are used as seeding material to obtain the mean and fluctuating velocity measurements for the continuous phase.

The turbulent Stokes number St_T, which is defined as the ratio of the particle response time to the fluid response time, characterizes the responsiveness of the particles to the fluid-phase turbulent fluctuations (Hardalupas et al., 1989). A value of St_T larger than one corresponds to unresponsive particles, with a value less than one corresponding to responsive particles

$$St_T = \frac{\tau_p}{\tau_f} \tag{3}$$

where τ_p and τ_f are the particle and fluid response time, respectively

$$\tau_p = \frac{d_p^2 \rho_s}{18\mu_f} \quad \text{and} \quad \tau_f = \frac{D}{U_{fz}} \tag{4}$$

where D is the pipe diameter, and U_{fz} is the fluid-phase mean axial velocity.

For both responsive and unresponsive particles, the convective motion of the particles is influenced by the mean motion of the fluid through the drag force. For unresponsive particles, however, the particle fluctuating motion does not simply follow the fluid fluctuations. The numerical studies of Simonin et al. (1997) and Yamamoto et al. (2001) indicate that particles of Stokes numbers greater than one engage in particle–particle collisions. These collisions greatly influence both the fluctuating motion and the radial distribution of these particles over the pipe cross-section even under very dilute conditions ($\upsilon \approx 10^{-4}$). These numerical studies have also recently been confirmed by the experimental studies of Caraman et al. (2003). The seeding particles used to measure the single-phase velocity in the present investigation have a St_T approximately equal to 0.3 and are highly responsive to the fluid velocity fluctuations. In contrast, the St_T values for the 70 and 200 μm glass beads ($\upsilon \approx 10^{-3}$) are significantly larger than one, which indicate that the particle motion for these particles is governed by particle–particle collisions.

The measurements reported in the present work are made at the exit of the pipe where the flow mimics the behavior inside the pipe. This is confirmed by comparing the single-phase measurements at the pipe exit with both turbulent pipe flow results as given by Schildknecht et al. (1979) and a single-phase low Reynolds number turbulence model by Myong and Kasagi (1990). Fig. 1 displays radial profiles of the axial mean velocity U_g and the axial fluctuating velocities u'_g for a single-phase flow in a pipe. The values of the mean and fluctuating velocities are

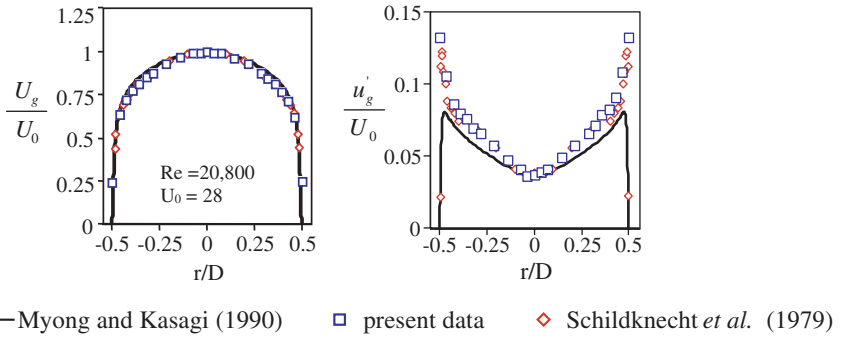

Fig. 1. Comparison of single-phase flow data at the pipe exit with the results of Schildknecht et al. (1979) and the k–ε turbulence model of Myong and Kasagi (1990) for fully developed, turbulent pipe flow.

normalized by the single-phase flow centerline mean velocity U_0. Fig. 1 shows an excellent agreement between the present data and the data of Schildknecht et al. (1979). The single-phase turbulence model predictions also agree with the measurements, except at the flow edges where the fluctuating velocities of the model are under-predicted due to the assumed isotropic velocity fluctuations in the k–ε model. In addition, two-phase flow measurements at the pipe exit from the present work were compared with the previous results of Hardalupas et al. (1989). The comparison between the velocity measurements from the present work for 70 μm particles ($Re = 13{,}800$, $m = 1.0$) and the velocity measurements from Hardalupas et al. (1989) for 80 μm glass beads ($Re = 13{,}000$, $m = 0.86$) is shown in Fig. 2. Excellent agreement exists between the results of the present work and those of Hardalupas et al. (1989).

A schematic of the flow system is displayed in Fig. 3. Particles from the storage hopper are mixed with air by means of a venturi eductor, and a pressure head is applied to the hopper to force a higher flow rate of exiting particles. The flow is then seeded with a reverse cyclone. The particle-laden flow transitions from a horizontal section of pipe through a 90° bend to the vertical nozzle with a length to diameter ratio of 100. The blind tee is necessary in order to redistribute the particles after the bend and 100 nozzle diameters are found to be adequate to obtain fully developed flow. The inside diameter of the smooth copper pipe is 1.42 cm and the jet expands into a 46 cm × 46 cm test chamber. A honeycomb straightener is located at the top of the test chamber to allow for the free entrainment of air from the surroundings by the expanding jet. Fans are located in the collection area at the bottom of the test chamber. These fans create a favorable pressure drop that aids the particles in exiting the test chamber. The fans entrain air from the surroundings at a maximum velocity of 0.06 m/s. The particles are collected in a container that sits on a load cell in order to calculate the particle loading by monitoring the steady flow of particles over the duration of an experimental run.

A two-component laser Doppler velocimetry/phase Doppler anemometry (LDV/PDPA) is used to make experimental measurements of the gas and particle mean and fluctuating velocities as well as the particle size. The optical system is composed of an argon ion laser (5 W), a Bragg cell unit creating a 40 MHz frequency shift in order to avoid directional ambiguity, transmitting and receiving optics, and a TSI/aerometrics real time signal analyzer. A traversing system with accuracy to within 1/10,000 of an inch is employed to explore the flow field. Table 1 summarizes the

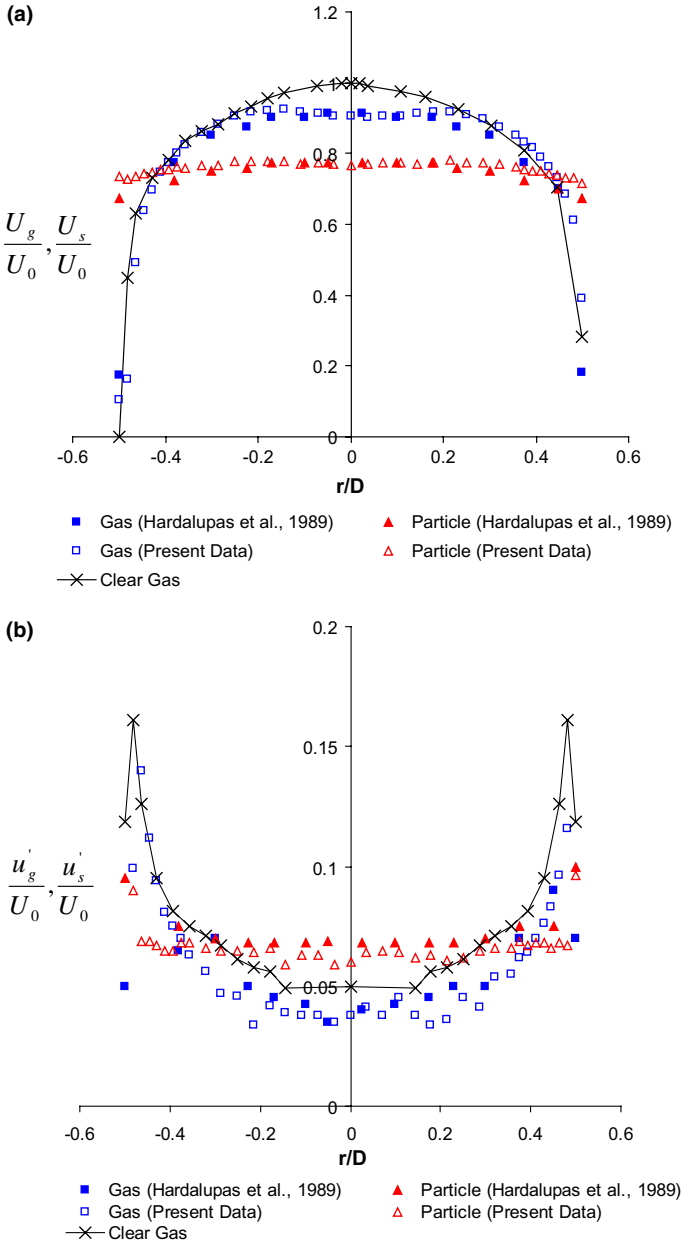

Fig. 2. (a) Comparison of two-phase axial mean velocity data (70 μm, $m = 1.0$, $Re = 13{,}800$) with the results of Hardalupas et al. (1989) (80 μm, $m = 0.86$, $Re = 13{,}000$) and (b) comparison of two-phase axial fluctuating velocity data (70 μm, $m = 0.1$, $Re = 13{,}800$) with the results of Hardalupas et al. (1989) (80 μm, $m = 0.86$, $Re = 13{,}000$).

relevant optical parameters of the LDV/PDPA. Two-phase measurements are made in two stages in order to measure the velocities of both the gas and the particles. The first stage involves making measurements of the gas in the presence of the particles. The high voltage for the photomultiplier

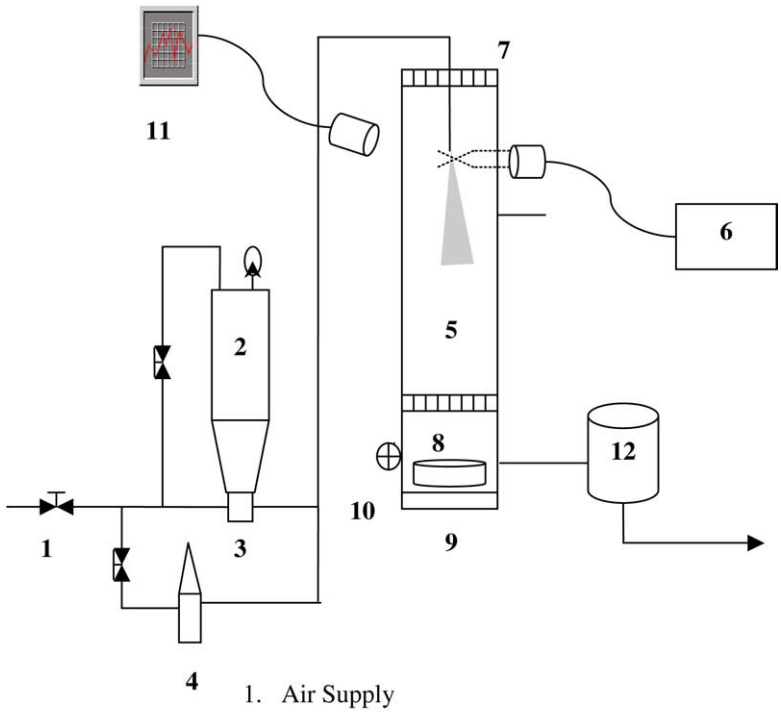

1. Air Supply
2. Particle Hopper
3. Venturi Eductor
4. Reverse Cyclone Seeder
5. Test Chamber
6. LDV/PDA
7. Honeycomb Flow Straightener
8. Particle Collection
9. Load Cell
10. Fans
11. Signal Processor
12. Filter

Fig. 3. Schematic diagram of the experimental facility.

tubes (PMTs) is set at a level just below the saturation point (350 V), and the burst threshold is set to 0.05 mV. In addition, the range for the particle size measurements of the PDPA in the first stage is set at less than 5 μm, so that only the velocity measurements of the seeding particles, which closely follow the gas motion, are included. In the present work, the limits for the burst threshold are chosen such that the experiments yield accurate particle size measurements while maintaining a constant sampling data rate throughout the process. The second stage involves measurements of the larger glass beads only. Here the PMTs are set to 250 V with a burst threshold of 0.3 mV. A higher burst threshold is necessary in order to minimize the inclusion of the seeding particles in the measurement samples. The range for the particle size measurements in the second stage is set to approximately 70 or 200 μm. A minimum of 1000 coincident samples is used for the measurements of both phases. Random errors in the measured velocities of the LDV/

Table 1
Optical parameters of the LDV/PDPA system

	Axial channel	Radial channel
Transmitting optics		
Wavelength (μm)	0.5145	0.488
Focal length (mm)	500	500
Beam separation (mm)	40	40
Laser beam diameter (mm)	1.4	1.4
Expander ratio	1	1
Fringe spacing (μm)	6.436	6.105
Beam waist (μm)	233.96	221.91
Length of volume (mm)	8.655	5.553
Frequency shift (MHz)	40	40
Receiving optics		
Focal length (μm)	521	
Slit aperture (μm)	50	
Collection angle	30°	

PDPA system are sensitive to the size of the ensemble used to calculate the measurements. Following the work of Yanta and Smith (1973), for a minimum of 1000 samples at 95% confidence level, the random errors in the mean and root mean square (RMS) velocities are less than 0.3% and 4.4%, respectively. In addition, random errors in the mean and fluctuating velocities due to experimental uncertainties in the particle loading are found on average (based on repeatability) to be 1–2% (mean) and 9–13% (RMS), respectively. The uncertainty analysis for the velocity measurements due to both the uncertainty in the particle loading and the LDV/PDPA sampling size is provided in Appendix A.

3. Results and discussion

In this section, measurements of the axial mean and fluctuating velocities of both the gas and particle phase, normalized by the single-phase centerline velocity U_0, are reported and analyzed. In some of the figures, the experimental data are connected by a line, intended solely to guide the eye. The particle loading is held constant at $m = 0.7$ and the Re is varied from 8300 to 23,700 for the 70 μm particles and from 6400 to 19,800 for the 200 μm particles. The Re calculation is based on the gas-phase superficial velocity. A summary of the experimental data, along with the turbulent Stokes numbers St_T and particle Reynolds numbers Re_p, is provided in Table 2. The St_T for both the 70 and 200 μm particles, over the range of Re investigated, are much greater than one, indicating the significant role of particle–particle collisions. The Re_p values, based on the slip velocity at the pipe center, are considerably less than 400, which indicate the absence of vortex shedding.

Figs. 4 and 5 display the changing relationship between the axial fluctuating velocities of the single-phase and two-phase flows as a function of Re for the 70 and 200 μm particles, respectively. For the 70 μm particles, the measurements were conducted at Re equal to 8300, 11,000, 13,800, 15,200, 16,600, 20,800 and 23,700. Detailed radial profiles, which present the key results, are

Table 2
Summary of experimental data

ρ_s (kg/m^3)	d_p (μm)	m	Re	St_T	Re_p
			8300	24	9
			11,000	32	5
			13,800	40	18
2500	70	0.7	15,200	44	18
			17300	50	20
			20,800	60	24
			23,700	68	28
			6400	148	28
			7200	168	40
			8000	186	44
2500	200	0.7	10,000	232	50
			12,200	284	61
			13,900	322	40
			15,500	360	48
			19,800	460	58

shown for Re equal to 8300, 13,800, 20,800, and 23,700. In Fig. 4a ($Re = 8300$), the axial fluctuating velocity of the single-phase flow u'_0 is greater than that of the gas phase in the presence of the particles u'_g over most of the pipe cross-section. The axial fluctuating velocity of the particles u'_s is also displayed in the figure and is larger than both u'_0 and u'_g at this Re. Gradually increasing Re affects the relationship between u'_0 and u'_g, as shown in Fig. 4b–d. The gas fluctuating velocity u'_g begins to exceed that of u'_0 for $Re > 13{,}800$ near the centerline. Furthermore, the axial fluctuating velocity of the gas begins to exceed that of the particles near the pipe center at $Re = 20{,}800$ (Fig. 4c), then exceeds the fluctuations of the particle phase over the entire pipe cross-section when $Re = 23{,}700$ (Fig. 4d).

For the 200 μm particles, experiments were conducted at Re equal to 6400, 7200, 8000, 10,000, 12,200, 13,900, 15,500 and 19,800. Similar to the 70 μm particles, the detailed profiles at selected Re (6400, 7200, 19,800) are displayed to present the key results. Fig. 5a shows that u'_g is approximately equal to u'_0, with both smaller than u'_s at $Re = 6400$. In Fig. 5b ($Re = 7200$), u'_g begins to increase near the centerline. At $Re = 19{,}800$ (Fig. 5c), u'_g is larger than both u'_0 and u'_s throughout the cross-section of the pipe.

Following the assumption of Gore and Crowe (1989)—that l_e is equal to $0.2R$ and independent of Re—the ratio d_p/l_e for the 70 and 200 μm particles in the present work is approximately 0.05 and 0.15, respectively. Hence, according to the criterion of Gore and Crowe (1989), gas turbulence should exhibit damping in the presence of the 70 μm particles. The present experimental data, however, indicate that is the case only for $Re < 13{,}800$. Hence, the experimental results indicate that consideration of the characteristic length scales alone, which are independent of Re, is not sufficient in predicting gas-phase turbulence modulation. These results also suggest that a better estimate for l_e, one not simply based on the pipe radius as in Gore and Crowe (1989), may be necessary for the Re range investigated in the present work. For the 200 μm particles, the experimental results, which indicate gas turbulence enhancement, are consistent with the prediction of Gore and Crowe (1989).

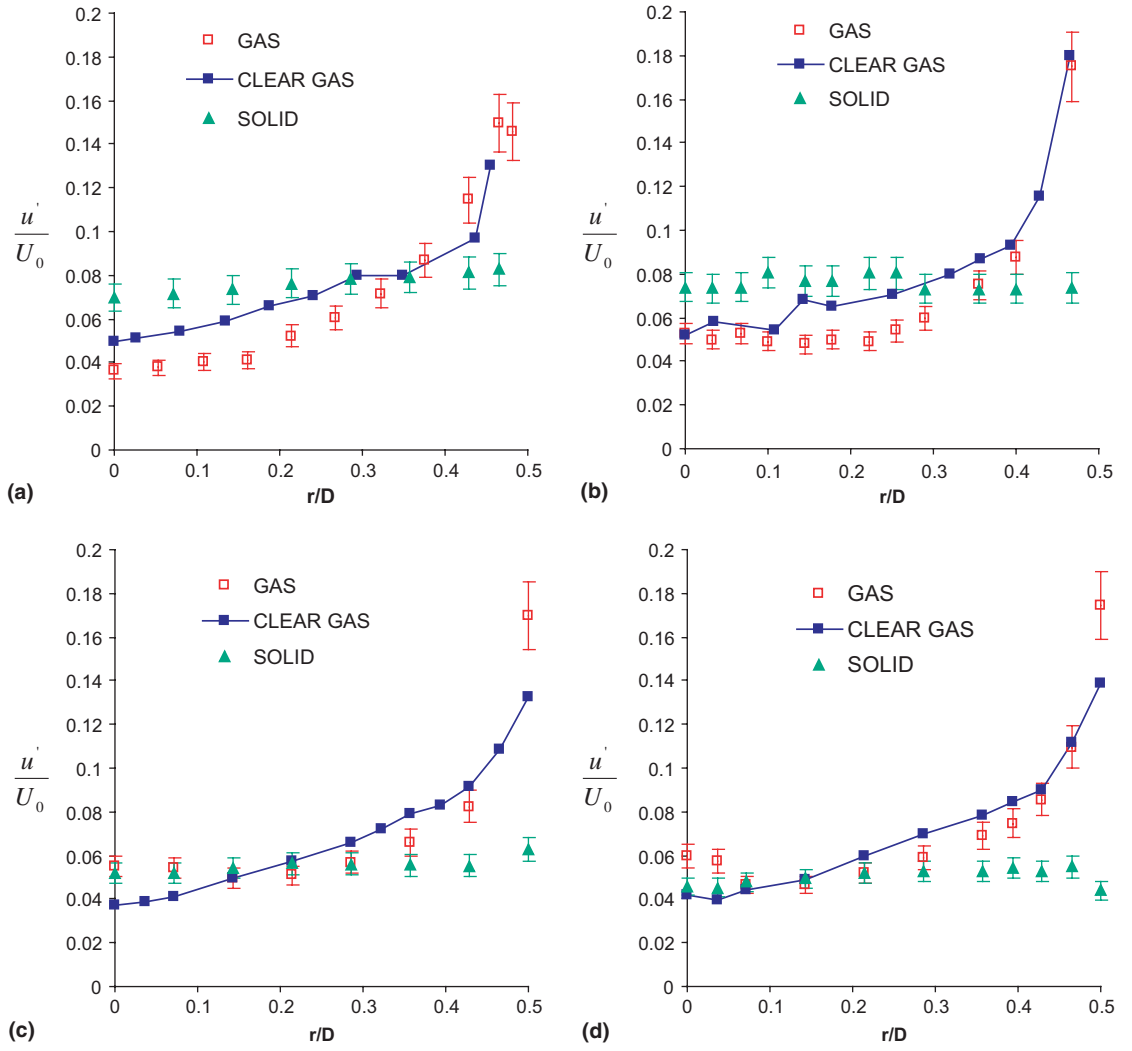

Fig. 4. Profiles of the axial fluctuating velocity at the pipe exit for the 70 μm particles: (a) $Re = 8300$; (b) $Re = 13{,}800$; (c) $Re = 20{,}800$ and (d) $Re = 23{,}700$.

As shown in Table 2, the maximum value for the Re_p, based on the slip velocity ($U_f - U_s$) at the pipe center, is 28 for the 70 μm particles and 61 for the 200 μm particles. As with the data of Maeda et al. (1980), these values are much lower than the criterion by Hetsroni (1989) as being necessary for vortex shedding and turbulence enhancement to occur. Hence, the present results, and the results of Maeda et al. (1980), suggest that some other mechanism must be responsible for the gas turbulence enhancement observed with the relatively small size particles at dilute loadings and at higher *Re* present in these experiments. A mechanism for the observed gas turbulence enhancement at high *Re* is postulated in the following discussion by considering changes in the radial solids segregation and the average volume fraction of the particles with increasing *Re*.

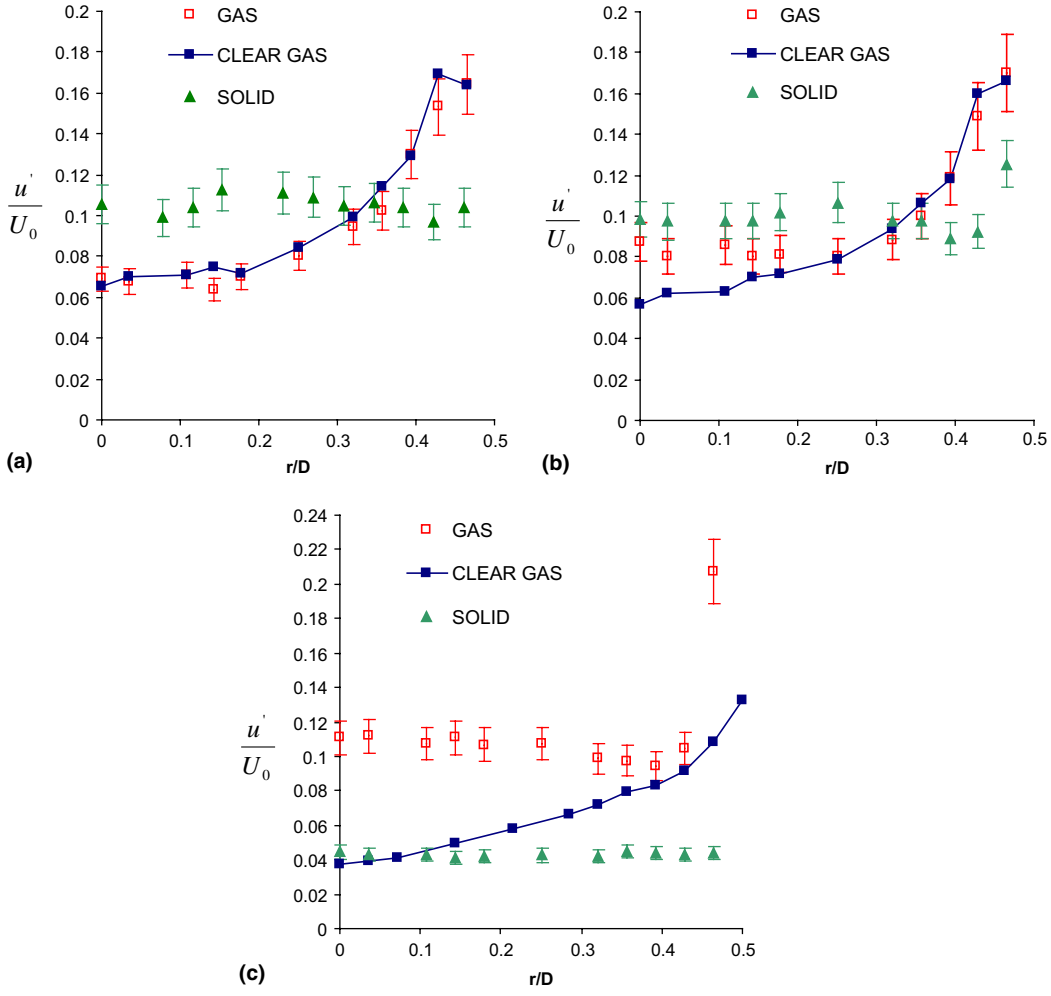

Fig. 5. Profiles of the axial fluctuating velocity at the pipe exit for the 200 μm particles: (a) $Re = 6400$; (b) $Re = 7200$ and (c) $Re = 19{,}800$.

Figs. 4 and 5 show the flattening of the fluctuating solid velocity profiles with increasing Re. For dilute-phase flow in a pipe with particles of high St_T, the particle fluctuating velocity is inversely related to the local particle volume fraction (Sinclair and Jackson, 1989). Therefore, the flattening of the u'_s profiles indicates that the particles become less segregated at higher Re, leading to a more uniformly distributed particle concentration over the pipe cross-section. This flattening, in turn, leads to a flattening of the fluctuating gas velocity profiles (Figs. 4 and 5), an outcome also reflected in the flattening of the mean gas velocity profiles with increasing Re (as shown in Figs. 6 and 7). The flattening of the U_g profiles indicates a more uniform distribution of the gas turbulence produced by shear over the pipe cross-section, implying that a larger fraction of the gas turbulence is diffused toward the centerline from the pipe wall at higher Re. It is postulated that this increased turbulence diffusion toward the pipe center at high Re is one of the principal mecha-

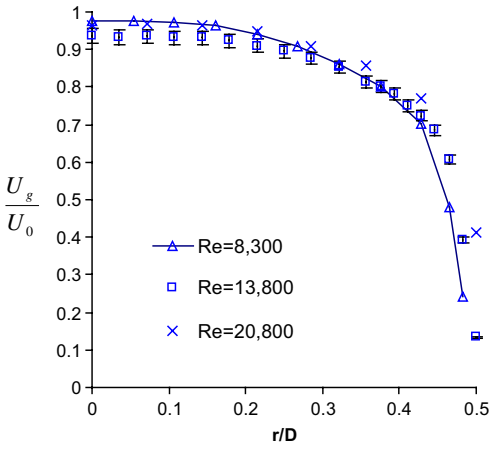

Fig. 6. Profiles of the axial mean velocity at different *Re* for the 70 μm particles.

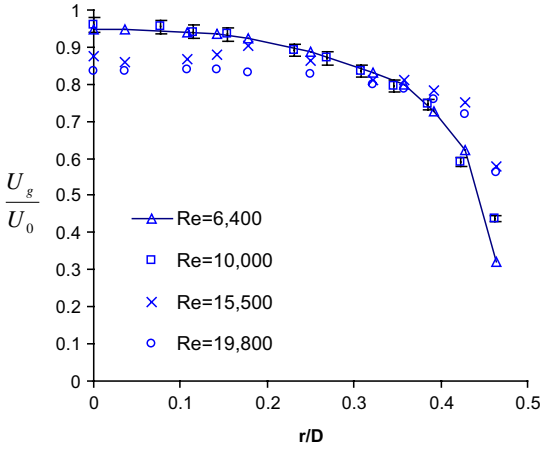

Fig. 7. Profiles of the axial mean velocity at different *Re* for the 200 μm particles.

nisms responsible for the gas turbulence enhancement observed in the presence of the smaller particles.

Figs. 8 and 9 give an overview of the observed trends in the axial fluctuating velocity by displaying centerline values for the particle phase, the clear gas (no particles), and the gas in the presence of particles as a function of *Re*. Values for the clear gas velocity fluctuations as given by a correlation of turbulence intensity with $Re(0.16/Re^{1/8})$ are also shown for comparison. The experimental data of the single-phase flow turbulence intensity are in agreement with the values predicted by the correlation over the range of *Re* investigated.

Figs. 8 and 9 show that, for both the 70 and 200 μm particles, the normalized particle axial fluctuating velocities at the centerline decrease, in general, with increasing *Re*. The decrease in the particle velocity fluctuations at the centerline with increasing *Re* can be explained by considering the

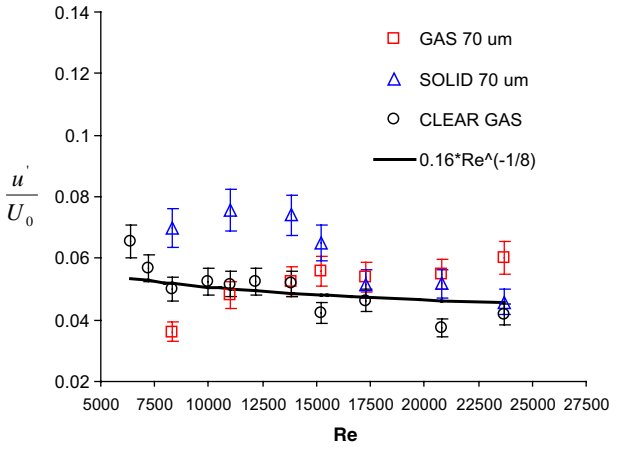

Fig. 8. Profiles of the axial fluctuating velocity at the pipe center as a function of *Re* for the 70 μm particles.

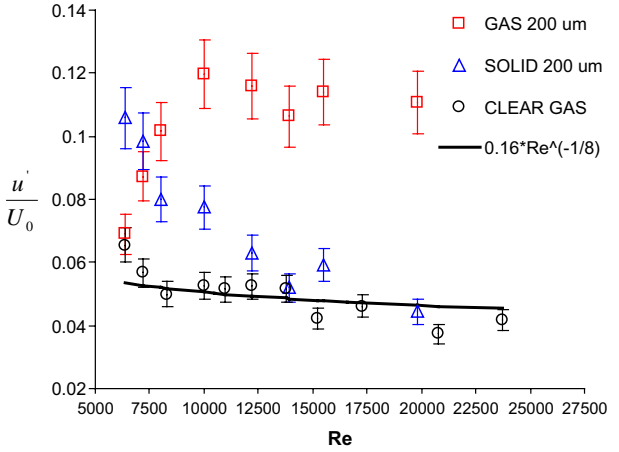

Fig. 9. Profiles of the axial fluctuating velocity at the pipe center as a function of *Re* for the 200 μm particles.

trend in the slip velocity as a function of *Re*. This trend, in turn, reflects the change in the average particle volume fractions with increasing *Re*. Figs. 10 and 11 show that the slip velocity normalized by the gas-phase axial mean velocity increases with increasing *Re* for both the 70 and 200 μm particles. Hence, the ratio of U_s to U_g decreases with increasing *Re*. Since the measurements were conducted at a constant particle loading, Eq. (1) implies that a decrease in the ratio $\frac{U_s}{U_g}$ must be accompanied by an increase in the average particle volume fraction to maintain a constant particle loading. Therefore, increasing the Reynolds number results in a higher average solids fraction and an increased frequency of particle collisions. Consequently, the magnitude of the particle velocity fluctuations decreases as particles engage in more inelastic collisions with each other and with the pipe wall.

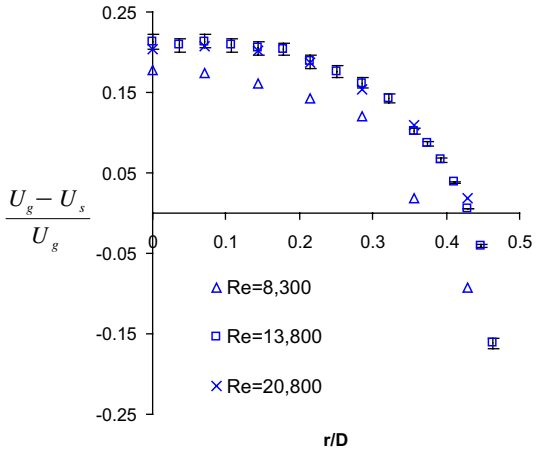

Fig. 10. Profiles of the normalized slip velocity at different *Re* for the 70 μm particles.

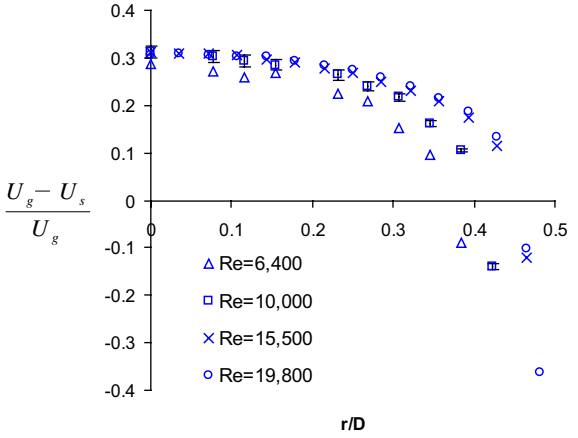

Fig. 11. Profiles of the normalized slip velocity at different *Re* for the 200 μm particles.

Figs. 8 and 9 also show that the normalized gas-phase fluctuating velocities at the centerline for both the 70 and 200 μm particles increase with increasing *Re*, eventually leading to gas turbulence enhancement at high *Re*. The gas turbulence enhancement at high *Re* in the absence of vortex shedding is postulated due to the aforementioned increase in the turbulence diffusion toward the pipe center with increasing *Re*. Based on the results shown in Figs. 10 and 11, this effect is thought to be coupled with a collective particle effect in which multiple neighboring particles moving with non-zero slip velocities enhance disturbances in the flow field. The collective particle effect will become more significant as the *Re* increases and the average volume fraction of the particles increase. Another possible contribution to the gas turbulence enhancement is the existence of particle rotation (Best, 1998) as a result of particle–particle collisions. This rotation effect will intensify with increasing solids volume fraction and increasing *Re*.

4. Conclusions

The experimental results presented in this study clearly indicate the important effect of *Re* on gas turbulence modulation for a given particulate material and solids loading. This effect has not yet been documented in the literature and helps to resolve some inconsistencies between previously published experimental data. Specifically, the experimental results for both the 70 and 200 μm particles indicate that the normalized gas velocity fluctuations increase with increasing *Re*, whereas the normalized particle velocity fluctuations decrease with increasing *Re*. In addition, the radial profiles of the velocity fluctuations for both the gas and solid phases flatten with increasing *Re*. It is postulated that the decrease in gas velocity fluctuations with increasing *Re* is a result of the combined influence of an increase in turbulence diffusion toward the pipe center and a collective particle effect. Particle rotation may also contribute to gas turbulence enhancement at higher *Re* due to an increase in the average particle volume fraction, and a subsequent increase in the particle collision frequency and decrease in the particle velocity fluctuations. Our experimental results have demonstrated that the demarcation criteria proposed by Gore and Crowe (1989) and Hetsroni (1989) for suppression or enhancement of gas turbulence in the presence of particles is inadequate to explain these and other previously published experimental results.

Acknowledgment

The authors would like to thank the American Chemical Society Petroleum Research Fund Grant# ACS-PRF#35117-AC9 for funding this work.

Appendix A. Uncertainty analysis

The intrinsic feature of the mean and fluctuating (RMS) velocities measurements reported in the present work is the uncertainty of those values due to both errors in the particle loading measurement and the random errors associated with the LDV/PDPA apparatus. Following the work of Yanta and Smith (1973), for a minimum of 1000 samples at 95% confidence, the errors in the mean and RMS velocities due to the uncertainty in the LDV/PDPA apparatus alone are at most 0.3% and 4.4%, respectively. The uncertainties due to the particle loading measurement are discussed next.

A.1. Uncertainty in particle loading m

Particle loading m is defined as the ratio of the particle mass flow rate m_p to the gas mass flow rate m_g.

$$m = f(m_p, m_g) = \frac{m_p}{m_g} \tag{A.1}$$

Thus, the uncertainty in the particle loading σ_{m} is, by definition, given as:

$$\sigma_{\mathrm{m}} = \sqrt{\sigma_{m_{\mathrm{p}}}^2 \left(\frac{\partial m}{\partial m_{\mathrm{p}}}\right)^2 + \sigma_{m_{\mathrm{g}}}^2 \left(\frac{\partial m}{\partial m_{\mathrm{g}}}\right)^2} \tag{A.2}$$

where

$$\frac{\partial m}{\partial m_{\mathrm{p}}} = \frac{1}{m_{\mathrm{g}}}; \quad \frac{\partial m}{\partial m_{\mathrm{g}}} = -\frac{m_{\mathrm{p}}}{m_{\mathrm{g}}^2} \tag{A.3}$$

Substituting Eq. (A.3) into Eq. (A.2)

$$\sigma_{\mathrm{m}} = \sqrt{\left(\frac{\sigma_{m_{\mathrm{p}}}}{m_{\mathrm{g}}}\right)^2 + \left(\frac{\sigma_{m_{\mathrm{g}}} m_{\mathrm{p}}}{m_{\mathrm{g}}^2}\right)^2} \tag{A.4}$$

The values of $\sigma_{m_{\mathrm{p}}}$ and $\sigma_{m_{\mathrm{g}}}$ are determined by the procedures described next.

A.1.1. Uncertainty in particle mass flow rate m_p

The particle mass flow rate is determined as follows:

$$m_{\mathrm{p}} = \frac{M_{\mathrm{p}}(t + \Delta t) - M_{\mathrm{p}}(t)}{\Delta t} = \frac{\Delta M_{\mathrm{p}}}{\Delta t} \tag{A.5}$$

where M_{p} and t are the mass of particles measured in the load cell and time, respectively.

Thus

$$\sigma_{m_{\mathrm{p}}} = \sqrt{\sigma_{\Delta M_{\mathrm{p}}}^2 \left(\frac{\partial m_{\mathrm{p}}}{\partial \Delta M_{\mathrm{p}}}\right)^2 + \sigma_{\Delta t}^2 \left(\frac{\partial m_{\mathrm{p}}}{\partial \Delta t}\right)^2} \tag{A.6}$$

$$\sigma_{\Delta M_{\mathrm{p}}} = \sqrt{2}\sigma_{M_{\mathrm{p}}} \quad \text{and} \quad \sigma_{\Delta t} = \sqrt{2}\sigma_t \tag{A.7}$$

Substituting Eq. (A.7) into Eq. (A.6) and calculating the derivatives

$$\sigma_{m_{\mathrm{p}}} = \sqrt{2\left[\left(\frac{\sigma_{M_{\mathrm{p}}}}{\Delta t}\right)^2 + \left(\frac{\sigma_t \Delta M_{\mathrm{p}}}{\Delta t^2}\right)^2\right]} \tag{A.8}$$

The random errors σ_t of the time measurements are estimated to be 2 s, the uncertainty of stopwatch usage. The measurements for the mass of particles have uncertainties attributed to both random errors and systematic errors. The values for the systematic and random errors in the load cell are found to be 0.055 and 0.100 lbs, respectively, by Budilarto (2003). Hence, $\sigma_{M_{\mathrm{p}}}$ is equal to 0.155 lbs.

A.1.2. Uncertainty in gas mass flow rate m_g

The volumetric flow rate of the gas Q_{g} is measured using a flow meter and a pressure gauge, and is determined as follows:

$$Q_g = Q_r(\text{scfm})\sqrt{1 + \frac{P(\text{psi})}{14.7}} \tag{A.9}$$

where Q_r and P are the gauge readings for the volumetric flow rate and pressure, respectively.

Thus,

$$\sigma_{Q_g} = \sqrt{\sigma_{Q_r}^2\left(\frac{\partial Q_g}{\partial Q_r}\right)^2 + \sigma_p^2\left(\frac{\partial Q_g}{\partial P}\right)^2} \tag{A.10}$$

Calculating the derivatives of Eq. (A.9) and substituting them into Eq. (A.10)

$$\sigma_{Q_g} = \sqrt{\sigma_{Q_r}^2\left(1 + \frac{P}{14.7}\right) + \left(\frac{\sigma_p Q_r}{29.4}\right)^2\left(\frac{14.7}{14.7 + P}\right)} \tag{A.11}$$

The errors in both instruments (the flowmeter and pressure gauge) are attributed to both random and systematic errors. According to Budilarto (2003), the random and systematic errors for the flowmeter are 0.02 and 0.05 scfm, respectively; the random and systematic errors for the pressure gauge are 0.5 and 1.2 psi, respectively. Hence, the respective values for σ_{Q_r} and σ_p are equal to 0.07 scfm and 1.7 psi. By assuming a constant gas density throughout the experiments at 1 atm and 298 K, one obtains

$$\sigma_{m_g} = \rho_f \sigma_{Q_g} \tag{A.12}$$

The values of σ_{M_p}, σ_t, σ_{Q_r}, σ_p have been determined, hence the values of σ_{m_p} and σ_{m_g} for an experimental run can be obtained from Eqs. (A.8), (A.11) and (A.12). Subsequently, the uncertainty in the particle loading measurement can be determined from Eq. (A.4).

A.1.3. Example of uncertainty analysis in particle loading m

The uncertainty analysis in the particle loading for experiments using glass beads at $Re = 8400$ and $m = 0.5$ is shown below.

$\sigma_{M_p} = 0.155$ lbs $\quad \sigma_t = 2$ s

$\sigma_{Q_r} = 0.07$ scfm $\quad \sigma_p = 1.7$ psi

Gas mass flow rate

$Q_r = 1.9$ scfm; $\quad P = 22$ psi; $\quad Q_g = 3$ scfm; $\quad m_g = 0.102$ kg/min

$\sigma_{Q_g} = 0.131$ scfm; $\quad \sigma_{Q_g} = 0.00371$ m^3/min; $\quad \sigma_{m_g} = 0.00445$ kg/min

Particle mass flow rate

Time (min)	Weight acc. (lbs)	Weight acc. (kg)	m_p (kg/min)	σ_{m_p} (lbs/min)	σ_{m_p} (kg/min)
5	0.6	0.27	0.0540	0.0438	0.0199
15	1.7	0.77	0.0513	0.0147	0.0067
30	3.4	1.55	0.0516	0.0073	0.0033
60	6.8	3.09	0.0515	0.0036	0.0016

Time (min)	m	σ_m	σ_m (%)
5	0.529	0.196	37.0
15	0.503	0.069	13.7
30	0.506	0.039	7.9
60	0.505	0.027	5.5

A.2. Uncertainty in mean and RMS velocities

All the experiments are conducted after a steady-state condition in particle loading is achieved, which occurs after about 15 min of elapsed time. Thus, as determined in the previous example, the uncertainties in the particle loading measurements range from 5% to 15%. These uncertainties, coupled with the uncertainties due to the LDV/PDPA apparatus, contribute to the uncertainties of the mean and RMS velocity measurements. The uncertainties of the velocity measurements for the experiments using the glass beads are determined by repeated measurements and are provided below.

Glass beads: 200 μm particles at $Re = 8000$, $m = 0.7$ and $Re = 10500$, $m = 0.7$

	$\frac{U_g}{U_0}, \frac{U_s}{U_0}$	$\frac{u'_g}{U_0}$	$\frac{u'_s}{U_0}$	$\frac{k}{U_0^2}$
σ(%)	1–2	9–13	9–13	14–15

The error bars displayed in the figures reflect these uncertainty values that are based on repeatability.

References

Best, J.L., 1998. The influence of particle rotation on wake stability at particle Reynolds numbers, $Re_p < 300$-implications for turbulence modulation in two-phase flow. Int. J. Multiphase Flow 24, 693–720.

Budilarto, S.G., 2003. An experimental study on effects of fluid aerodynamics and particle size distribution in particle-laden jet flows. Ph.D. Thesis, Purdue University, West Lafayette, IN.

Caraman, N., Boree, J., Simonin, O., 2003. Effect of collisions on the dispersed phase turbulence in a dilute tube flow: experimental and theoretical analysis. Phys. Fluids 15, 3602–3612.

Gore, R.A., Crowe, C.T., 1989. Effect of particle size on modulating turbulent intensity. Int. J. Multiphase Flow 15, 279–285.

Hardalupas, Y., Taylor, A., Whitelaw, J., 1989. Velocity and particle–flux characteristics of turbulent particle-laden jets. Proc. R. Soc. London A 426, 31–78.

Hetsroni, G., 1989. Particle–turbulence interaction. Int. J. Multiphase Flow 15, 735–746.

Hutchinson, P., Hewitt, G., Dukler, A.E., 1971. Deposition of liquid or solid dispersion from turbulent gas streams: a stochastic model. Chem. Eng. Sci. 26, 419–439.

Kulick, J.D., Fessler, J.R., Eaton, J.K., 1994. Particle response and turbulence modification in fully developed channel flow. J. Fluid Mech. 277, 109–134.

Lee, S.L., Durst, F., 1982. On the motion of particles in turbulent duct flows. Int. J. Multiphase Flow 8, 125–146.

Maeda, M., Hishida, K., Furutani, T., 1980. Optical measurements of local gas and particle velocity in an upward flowing dilute gas–solids suspension. Polyphase Flow Transport Technology, Century 2-ETC, San Francisco, CA.

Myong, H., Kasagi, N., 1990. A new approach to the improvement of k–ε turbulence model for wall-bounded shear flows. JSME Int. J. 33, 63–72.

Schildknecht, M., Miller, J., Meier, G., 1979. The influence of suction on the structure of turbulence in fully developed pipe flow. J. Fluid Mech. 90, 67–107.

Simonin, O., Wang, Q., Squire, K.D., 1997 Comparisons between two-fluid model predictions and large eddy simulation results in a vertical gas–solid turbulent channel flow. In: Proceedings of the 7th International Symposium on Gas–Particle Flows, ASME, FEDSM'97-3625.

Sinclair, J.L., Jackson, R., 1989. Gas–particle flow in a vertical pipe with particle–particle interactions. AICHE J. 35, 1473–1486.

Tsuji, Y., Morikawa, Y., Shiomi, H., 1984. LDV measurements of an air–solid two-phase flow in a vertical pipe. J. Fluid Mech. 139, 417–434.

Yamamoto, Y., Potthoff, M., Tanaka, T., Kajishima, T., Tsuji, Y., 2001. Large eddy simulation of turbulent gas–particle flow in a vertical channel: effect of considering interparticle collisions. J. Fluid Mech. 442, 303–334.

Yanta, W., Smith, R., 1973. Measurements of turbulence transport properties with a Laser Doppler Velocimeter, AIAA 11th Aerospace Sciences Meeting, AIAA Paper No. 73-169, Washington, DC.